Available online at www.sciencedirect.com
ScienceDirect
Journal of Power Sources 175 (2008) 68–74
JOURNAL OF POWER SOURCES
www.elsevier.com/locate/jpowsour

Development of cube-type SOFC stacks using anode-supported tubular cells

Toshio Suzuki [a,*], Yoshihiro Funahashi [b], Toshiaki Yamaguchi [a], Yoshinobu Fujishiro [a], Masanobu Awano [a]

[a] *National Institute of Advanced Industrial Science and Technology (AIST), 2266-98 Anagahora, Shimo-Shidami, Moriyama-ku, Nagoya 463-8560 Japan*
[b] *Fine Ceramics Research Association (FCRA), 2266-98 Anagahora, Shimo-Shidami, Moriyama-ku, Nagoya 463-8560 Japan*

Received 23 July 2007; received in revised form 4 September 2007; accepted 21 September 2007
Available online 2 October 2007

Abstract

Tubular SOFCs have shown many desirable characteristics such as high thermal stability during rapid heat cycling and large electrode area per unit volume, which can accelerate to realize SOFC systems applicable to portable devices and auxiliary power units for automobile. So far, we have developed anode-supported tubular SOFCs with 0.8–2 mm diameter using Gd-doped CeO_2 (GDC) electrolyte, NiO-GDC anode and (La, Sr)(Co, Fe)O_3 (LSCF)-GDC cathode. In this study, a newly developed cube-type SOFC stack which consists of three SOFC bundles was designed and examined. The bundle consists of three 2 mm diameter tubular SOFCs and a rectangular shaped cathode support where these tubular cells are arranged in parallel. The performance of the stack whose volume is less than 1 cm^3 was shown to be 2.8 V OCV and over 1 W at 1.6 V under 500 °C. Cathode loss factor due to current collection from cathode matrix was also estimated using a proposed model.

Keywords: SOFC; Tubular; Cube; Ceria; Anode-supported; Stack

1. Introduction

Use of solid oxide fuel cells (SOFCs) have been considered as one of solutions for environmental issues and many efforts poured into the development of SOFCs for commercialization [1,2]. A typical SOFC consists of doped zirconia for electrolyte, Ni cermet for anode and doped lanthanum manganite for cathode, and it was shown its long-term stability over 20,000 h operation as well as high power output up to 2 W cm^{-2} at 800 °C [3–5].

Currently, decrease of operating temperature under 700 °C becomes one of main research targets because it can decrease material degradation, prolong stack lifetime, and reduce cost by utilizing metal materials for stack fabrication. Therefore, number of studies related to reduced temperature SOFCs have been reported. The approaches to reduce operating temperature have widely been reported: for example (1) using a new electrolyte, cathode and anode materials [6–14], (2) reducing the thickness of the electrolyte using traditional electrolyte materials such as Y-doped ZrO_2 [4,15], and (3) introducing new structure for electrolytes [16–18].

Cell design is also an important factor to improve the performance of SOFC stack/module. Tubular design was the first introduced one for commercialized SOFC by Siemens Westinghouse, and then, tubular SOFCs were well investigated from fundamental consideration to stack modulation using anode-supported tubular design up to several kW scale stacks [19,20].

Further improvement of SOFCs system may be achieved by use of small-sized tubular SOFCs, since it was shown that high mechanical strength during rapid start up operation [21,22]. Use of small diameter SOFC may also give opportunity to reduce operating temperature by increasing the volumetric power density [23]. Thus, they are expected to accelerate the progress of

* Corresponding author. Tel.: +81 52 736 7295; fax: +81 52 736 7405.
E-mail address: toshio.suzuki@aist.go.jp (T. Suzuki).

0378-7753/$ – see front matter © 2007 Elsevier B.V. All rights reserved.
doi:10.1016/j.jpowsour.2007.09.082

SOFC systems, which can be applied to portable devices and auxiliary power units for automobile.

Our study aims to develop fabrication technology for small-sized tubular SOFCs and their stacks. So far, we have developed anode-supported tubular SOFCs with various diameter ranging from 0.8 to 2 mm using Gd-doped CeO_2 (GDC) electrolyte, NiO-GDC anode and (La, Sr)(Co, Fe)O_3 (LSCF)-GDC cathode. The performance of these cells are sufficiently high, ranging from 0.17 to 0.48 W cm^{-2} at 0.7 V at the operating temperature of 450–550 °C [24]. Therefore, the key for further development lies on the design and fabrication technology of the bundles and stacks for the tubular SOFCs.

In this study we proposed a newly designed, cube-type SOFC stack consists of three bundles using 2 mm diameter tubular cells and porous cathode matrices as supports of the tubular cells. The stack was designed by optimizing the property of the cathode matrix, whose microstructure and electrical conductivity were investigated as functions of various preparation parameters. Cathode loss factor (current collecting loss due to cathode matrix) as a function of cell configuration in the cathode matrix was calculated using a model to design highly efficient cube-type SOFC stacks. The stack performance test was conducted to seek the possibility of application of SOFCs in the temperature range under 500 °C.

2. Experimental

Fig. 1 shows the processing procedure of the tubular SOFCs and their bundles. Anode tubes were made from NiO powder (Seimi Chemical Co. Ltd.), $Gd_{0.2}Ce_{0.8}O_{2-x}$ (GDC) (Shin-Etsu Chemical Co. Ltd.), polymethyl methacrylate beads (PMMA) (Sekisui Plastics Co. Ltd.), and cellulose (Yuken Kogyo Co. Ltd.). After adding proper amount of water, these powders were mixed using a mixer 5DMV-rr (Dalton Co. Ltd.) in a vacuumed chamber. The tubes were extruded from the clay using a piston cylinder type extruder (Ishikawa-Toki Tekko-sho Co. Ltd.) with a metal mold of out Ø 2.4 mm–in Ø 2.0 mm.

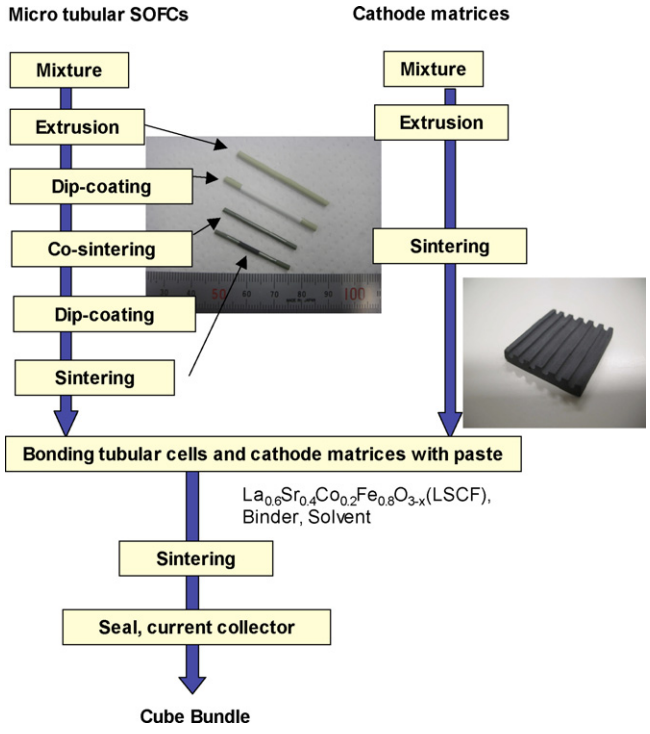

Fig. 1. Fabrication process of the tubular SOFCs, cathode matrices, and bundles.

An electrolyte was prepared on the surface of the anode tube by dip-coating a slurry which consists of the GDC powder used in the anode tube preparation, solvents (methyl ethyl ketone and ethanol), binder (polyvinyl butyral), dispersant (polymer of an amine system) and plasticizer (dioctyl phthalate), and co-sintered at 1400 °C for 1 h in air. Typical thickness of the electrolyte layer is around 20 μm after sintering. The diameter of the tube after sintering was 2 mm. A cathode was also prepared by dip-coating the slurry of $La_{0.6}Sr_{0.4}Co_{0.2}Fe_{0.8}O_{3-y}$ (LSCF) powder (Seimi Chemical Co. Ltd.), the GDC powder, and organic ingredients. Fig. 1 (left) also shows the image of a green tube, a green tube with dip-coated electrolyte, a sintered tube with electrolyte, and a complete cell, respectively.

A cathode matrix was proposed to bundle the tubular SOFCs as shown in Fig. 1 (right). The cathode matrix was made from LSCF powder (Daiichi Kigenso Kagaku Kogyo Co. Ltd.), polymethyl methacrylate beads (PMMA) and cellulose (Yuken Kogyo Co. Ltd.). Three different particle sizes of the LSCF powders (0.05, 2, 20 μm, respectively) was used to investigate the effect on the microstructure as well as the electrical property. These powders were mixed and extruded from a metal mold using a screw cylinder type extruder (Miyazaki Tekko Co. Ltd.). The microstructure of the cathode matrices was controlled by changing the amount and diameter of pore-former, the grain size of starting LSCF powder and sintering temperatures [25].

For connecting tubular SOFCs and cathode matrices, a bonding paste was used, prepared by mixing the LSCF powder, the binder (cellulose), the dispersant (polymer of an amine system), and the solvent (diethylene glycol monobutyl ether). The paste was screen-printed on the surface of the cathode matrices, followed by the placement of the tubular cells and sintered at 1000 °C for 1 h in air. Afterwards, an insulator, glass seal, anode current collector (Ag paste and sheet) was applied to complete the bundle with electrical connectors.

A schematic image and a photo of the stack made of three SOFC bundles are shown in Fig. 2(a) and (b). Since each bundle has current collectors for anode (attached on the top of the bundle) and for cathode (whole bottom area of the bundle) as shown in Fig. 2(a), it allows simple assemble of stacks in series electrical connection. In addition, an inserted image in Fig. 2(b) shows good quality of connection between tubular cell and the cathode matrix. Since the thickness of the connection layer is much smaller than the electrical path in the porous cathode, the influence of the connection layer is considered to be very small.

The stack performance test was conducted using the experimental setup shown in Fig. 3. Thermocouples were placed at the inlet and outlet of each gas, and at the bottom of the stack. The discharge characterization was investigated by using a Parstat 2273 (Princeton Applied Research) in DC 4-point probe measurement. The Ag wire was used for collecting current from anode and cathode sides, which were both fixed by Ag paste.

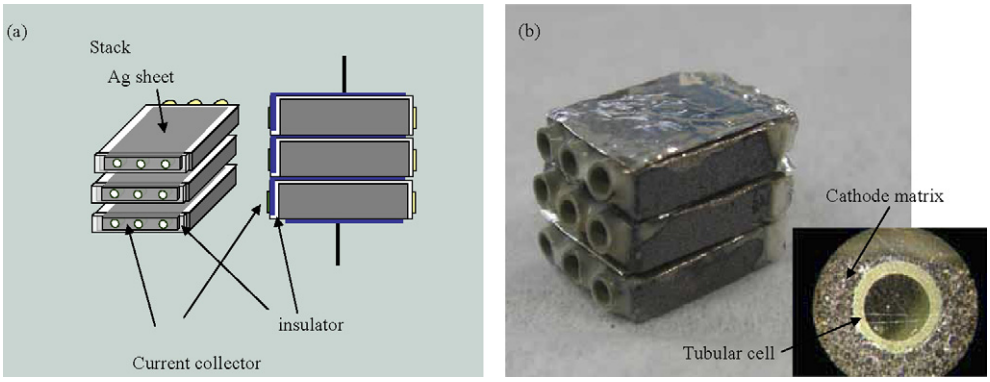

Fig. 2. (a) A schematic image of the tubular SOFC stack (three bundles in series) and (b) an image of actual tubular SOFC stack with the volume of less than 1 cm^3 with an image of tubular cell–cathode matrix connection.

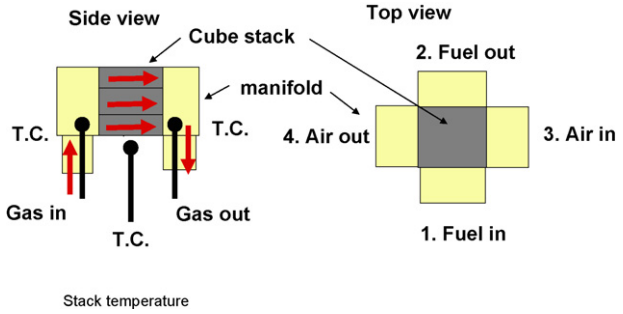

Fig. 3. Experimental setup for stack performance test.

Hydrogen (humidified by bubbling water at room temperature) was flowed at the rate of 100 mL min^{-1} and the air was flowed at the rate of 1000 mL min^{-1} at the cathode side.

3. Calculation

3.1. Estimation of cathode loss factor due to the resistance of cathode matrix

Because the cathode matrix, which connects the tubular cell and a current collector from a neighbouring bundle, is used as current path, it is important to estimate the loss of cell performance due to the resistance of the cathode matrix. The influence of the cathode matrix becomes significant, especially when the porosity of the cathode matrix and/or the packing density of the tubular cells increase, in other words, the current path in the cathode matrix is reduced. We have already reported that the performance loss due to current collection from the edge of the anode tube could be significant, which was concluded that it is important to optimize the size (tube length and anode tube thickness) [26].

I–V characteristic of the cell can be given as

$$V = E_0 - IR_T, \tag{1}$$

where V, I, E_0, R_T are terminal voltage, current density, the open circuit voltage of the cell and the total cell resistance (area specific resistance of the cell), respectively. R_T is typically not constant and changes depending upon operating conditions. In this calculation, however, R_T was calculated from the current density where the maximum power density is obtained. Around this region, R_T is considered to be constant, and then, R_T was separated to

$$R_T = R_{cell} + R_{cathode}, \tag{2}$$

where R_{cell} and $R_{cathode}$ are the cell resistance and the resistance of the cathode matrix, respectively, to estimate the effect of cathode matrix as a current collector. By applying Eq. (2) to (1), following relation is obtained:

$$V = E_0 - I(R_{cell} + R_{cathode}) = E_0 - IR_{cell}\left(1 + \frac{R_{cathode}}{R_{cell}}\right)$$
$$= E_0 - IR_{cell}(1 + \beta). \tag{3}$$

Here, the cathode loss factor, β, is defined as the ratio of $R_{cathode}$ and R_{cell},

$$\beta = \frac{R_{cathode}}{R_{cell}} = \frac{(R_T - R_{cell})}{R_{cell}}. \tag{4}$$

By calculating R_{cell} and β, it is possible to estimate the voltage drop (performance loss) due to the resistance of the cathode matrix.

Here, attempts were made to estimate the effect of cathode matrix, defined as β using the following calculation model. Fig. 4(a) shows the cross-sectional schematic image of the tubular SOFC bundle for calculation; a current collector was attached at the bottom of the bundle (see Fig. 2(a)). In this model, the current flow in the tubular cell was assumed to be constant and uniform. Using the symmetrical configuration of the tubular cells in the cathode matrix, and the current collector, the model can be simplified and half of single cell in the bundle was extracted for further calculation. As can be seen in Fig. 4(b), the total resistance includes the resistance of the cell as well as the cathode matrix.

In this calculation model, the cathode matrix and the anode tubes were sliced with the thickness of Δx as shown in Fig. 4(b). As can be seen, each slice consists of the tubular cell and the cathode matrix in series, then, each slice is connected in parallel and therefore an equivalent circuit as shown in Fig. 4(c) was set up to estimate the total bundle resistance including cell and cathode matrix resistances, assuming that the cell parts have equal potential distribution. Number of division, N, was set to 60,000.

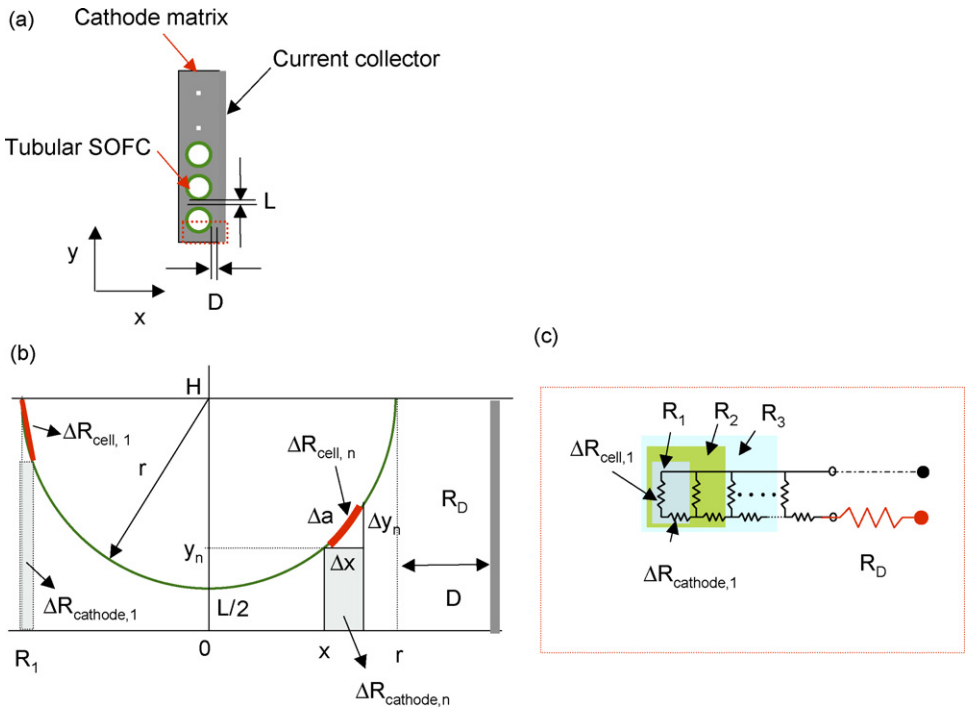

Fig. 4. (a) A schematic image of the tubular SOFC bundle, (b) a calculation model of the bundles and calculating area, and (c) an equivalent circuit of the model for calculation.

$\Delta R_{\text{cell},n}$ and $\Delta R_{\text{cathode},n}$ shown in Fig. 4(b) are the resistance of the tubular cell and the cathode matrix in the slice, respectively. $R_1, R_2, \ldots, R_N$ shown in Fig. 4(c) were given by following equations:

$$\begin{aligned} R_1 &= \Delta R_{\text{cell},1} + \Delta R_{\text{cathode},1} \\ R_2 &= \frac{(\Delta R_{\text{cell},1} R_1)}{(\Delta R_{\text{cell},1} + R_1)} + \Delta R_{\text{cathode},2} \\ &\vdots \\ R_{N-1} &= \frac{(\Delta R_{\text{cell},N-2} R_{N-2})}{\Delta R_{\text{cell},N-2} + R_{N-2}} + \Delta R_{\text{cathode},N-1} \\ R_N &= \frac{(\Delta R_{\text{cell},N-1})}{(\Delta R_{\text{cell},N-1} + R_{N-1})} + \Delta R_{\text{cathode},N} \end{aligned} \tag{5}$$

where R_N is the calculated total resistance determined from Eq. (5). $\Delta R_{\text{cathode},n}$ was obtained from following equations:

$$\Delta R_{\text{cathode},n} \sim \frac{\Delta x}{(y_n \sigma)} \tag{6}$$

where $y_n = \mathrm{H} - (r^2 - x^2)^{1/2}$. σ is the conductivity of the cathode shown in Table 1. ΔR_{cell} can be calculated from:

$$\Delta R_{\text{cell},n} = \frac{R_{\text{cell}}}{\Delta a_n}. \tag{7}$$

As shown in Fig. 4(b), Δa is approximately given as $\Delta a_n \sim ((\Delta x)^2 + (\Delta y_n)^2)^{1/2}$ and Δy_n was described as

$$\Delta y_n \sim \Delta_x \left(\frac{x}{(r^2 - x^2)^{1/2}} \right). \tag{8}$$

Now Δa_n is rewritten as shown below:

$$\Delta a_n \sim \Delta x \left(\frac{r}{(r^2 - x^2)^{1/2}} \right). \tag{9}$$

The error of this approximation was estimated to be less than 0.4% when $N = 60{,}000$. In this calculation, as mentioned before, the current collecting resistance of the anode part was

Table 1
Properties of the cathode matrix prepared from various LSCF powders with different grain size

	LSCF0.05	LSCF2	LSCF20
Grain size of LSCF (μm)	0.05	2	20
Porosity (%)	60.7	68.6	78.2
Gas permeability (mL cm cm^{-2} s^{-1} Pa^{-1}) at 400 °C	8.5×10^{-6}	8.4×10^{-5}	6.2×10^{-4} 57.1
Conductivity (S cm^{-1})			
At 500 °C	139	108	57.6
At 600 °C			56.2

Amount of PMMA 70 vol.%. Sintering temperature: 1400 °C.

not included and separately discussed elsewhere [26]. To calculate β, R_{cell} needs to be calculated which is implicitly included in Eq. (7) using the experimental value, R_T. Thus, the determination of R_{cell} was made by varying R_{cell} so that the calculated total resistance, R_N, becomes equal to R_T.

4. Results and discussion

4.1. Gas permeability and electrical conductivity of the cathode matrix

Table 1 shows the property of the cathode matrices prepared from different LSCF powders with grain sizes, 0.05, 2, and 20 μm, and each sample was named as LSCF0.05, LSCF2 and LSCF20, respectively. As can be seen, the microstrucure of the cathode matrix can be effectively controlled by changing the grain size of starting material. The porosity varied from 60 to 78%, corresponding to the variation of gas permeability from 8.5×10^{-6} to 6.2×10^{-4} mL cm cm^{-2} s^{-1} Pa^{-1}. The electrical conductivity of the LSCF20 specimen was ranged from 56.2 to 57.1 S cm^{-1} at between 400 and 600 °C due to high porosity of the specimen, which were far lower than bulk conductivity ~ over 300 S cm^{-1} [27].

Fig. 5 shows the relationship between maximum gas flow obtained in the cathode matrices under given pressure differences (0.01–0.03 MPa) and the gas permeability for samples in Table 1. As can be seen, under given pressure difference, only LSCF20 can be used to obtain sufficient gas (air) flow to achieve 2 W cc^{-1} (dashed line in Fig. 5), which is our target volumetric power density, assuming that air utilization is 30%. These results suggested that a compressor may be needed to feed air when LSCF2 and LSCF0.05 were used to gain higher electrical conductivity for current collecting. The effect of the electrical conductivity of the cathode matrix will be discussed later using the calcuration model.

4.2. Performance of cube-type SOFC stacks

Fig. 6 shows initial start up behavior of the stack started at 385 °C stack temperture. As can be seen, even at under 400 °C, the stack can be started without reducing anode at higher temperture, and showed over 2.8 V around after 10 min. Maximum OCV obtained in this stack (three bundles in series connection) was 2.85 V (0.95 V per bundle), which was lower than theoretical OCV value of a single cell (bundle) is around 1.14 V at 500 °C, thus, 3.42 V for three bundle stacks [28]. It can be said that lower OCV was resulted from the use of ceria-based electrolyte [28–30], and compared to those literatures, OCV obtained for the ceria-based SOFC stack was a reasonable value. Several efforts were made to overcome this problem, such as use of an interlayer inside ceria electrolyte to block the leak current [31]. On the other hand, there is a report that the leak current can be cancelled out during cell operation [32]. This means that the efficiency drop due to use of ceria-based electrolyte can be minimized by optimizing the operating conditions as well as the design of a SOFC system.

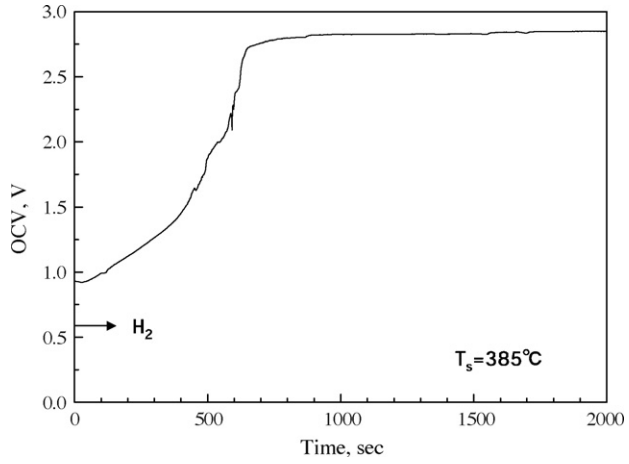

Fig. 6. Initial start up behavior of the tubular SOFC stack (three bundles in series) at 385 °C.

Table 2
Temperatures of each experimental point during stack operation

Stack temperature (°C)	1	2	3	4
385	381	388	385	415
423	424	432	433	460
484	485	512	492	521

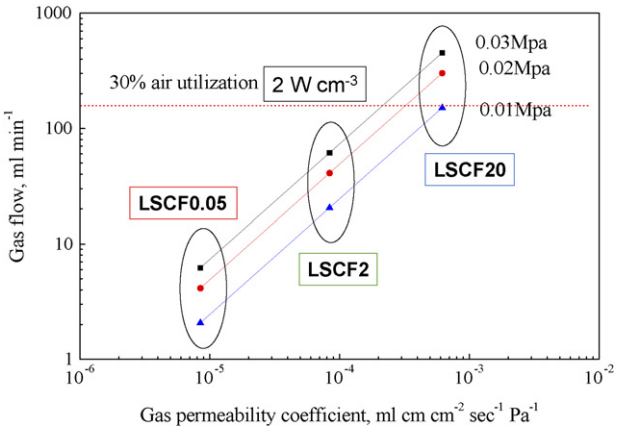

Fig. 5. The gas flow in the cathode matrices as a function of gas permeability estimated for LSCF0.05, LSCF2, and LSCF20.

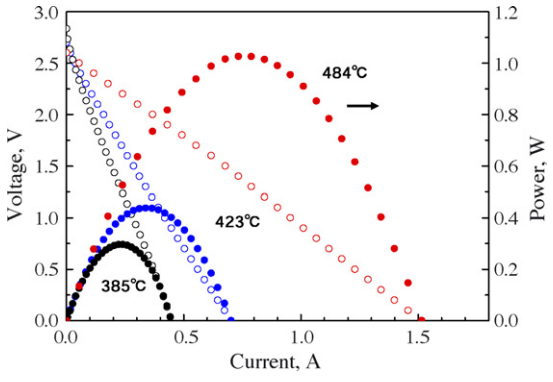

Fig. 7. Performance of the SOFC stack operated from 385 to 484 °C.

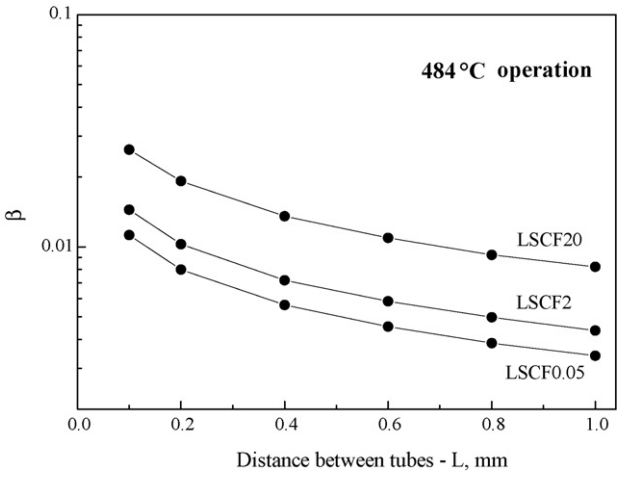

Fig. 8. Results of calculation for the cathode loss factor obtained for LSCF0.05, LSCF2, and LSCF20 at 484 °C operating temperature. The values of the cathode conductivity were chosen from Table 1.

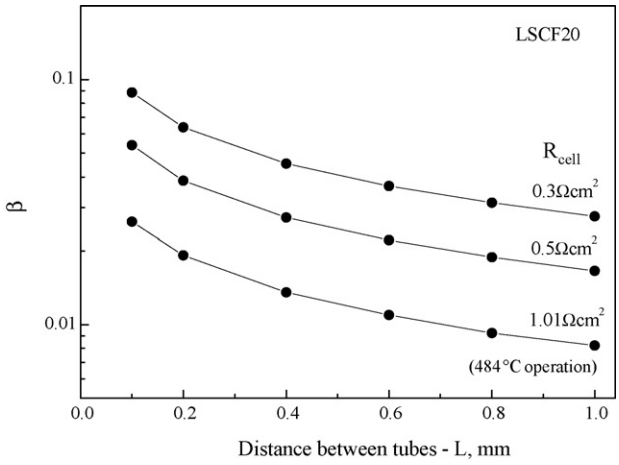

Fig. 9. Results of calculation for the cathode loss factor obtained for LSCF20 cathode matrix at different R_{cell}.

Table 2 shows the temperature of each measurement point in Fig. 3 at various stack temperatures. As can be seen, outlet gas temperaure is always higher due to increase of temperare inside the stack. Currently, temperature distribution and gas flow inside the cathode matrices are under investigation using simulation to optimaize the design of the stack.

Fig. 7 shows the performace of the stack with the volume of less than 1 cc. The maximum output powers of 0.3, 0.44, 1.0 W were obtained for 385, 423, 484 °C stack tempertures, respectively. These results indicated that a portable SOFC system operable under 500 °C, even under 450 °C can be realized using the developed tubular SOFC stacks. Total electrode area of the tubular SOFCs is 5.65 cm^2 and thus, the power density of 0.18 W cm^{-2} was obtained at 484 °C operating temperature. In fact, this was lower than that of the single cell, and thus, further improvement of the stack performance can be expected by optimizing gas flow rates, interfacial resistance of the tubular SOFC, as well as improving the cathode matrix and sealing technology.

4.3. Estimation of cathode loss factor for the tubular SOFC stack

The values of R_T determined to be 1.02 Ωcm^2 at around the maximum power output region at the operaing condition 484 °C using Eq. (1). Note that this value was estimated for single bundle (three tubular cells; total electrode area 1.88 cm^2) using the expermental results obtained for the three bundle stack as shown in Fig. 7, assuming that each bundle performance is the same.

Fig. 8 shows the cathode loss factor, β, as a function of distance between tubes as shown in Fig. 4(a) at the operaing condition 484 °C for the cathode matrices, LSCF20, LSCF2 and LSCF0.05, respectively ($r = 1$ mm, $D = 1$ mm). First, the R_{cell} was estimated using the experiemtal value, R_T (using LSCF20 cathode martix), to be 1.01 Ωcm^2. Then, using the estimated R_{cell}, β's for LSCF2 and LSCF0.05 were calculated.

As can be seen in Fig. 8, β directly influenced by the distance between tubes. β was estimated to be less than 0.01 for all cathode matrices using current tubular cell configuration ($L = 1$ mm). It also shows that use of LSCF0.05 can reduce β effectively

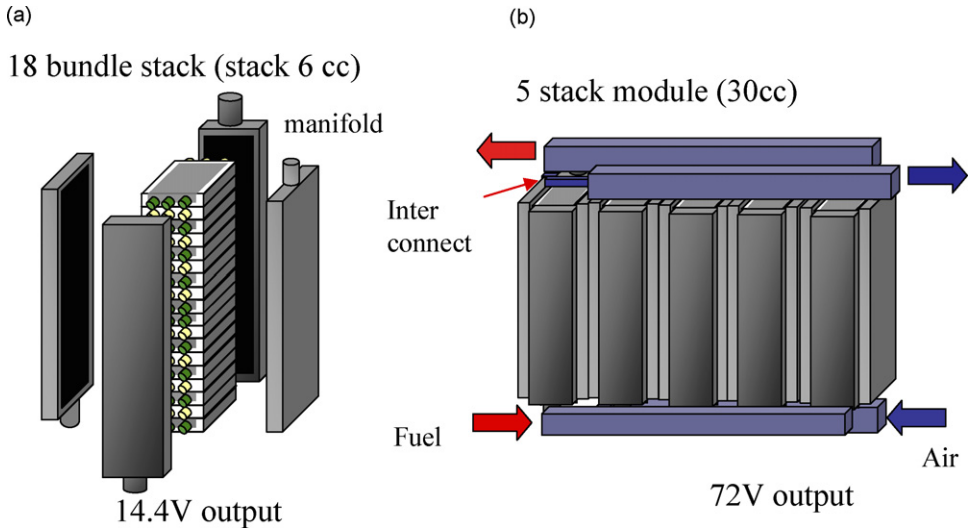

Fig. 10. Schematic images of stacks and modules using the tubular SOFC bundles.

for lower L, in turn, further accumulation of tubular cells in the cathode matrices to obtain higher volumetric power density. On the other hand, it should be noted that use of LSCF2 and LSCF0.05 may lead to significant performance loss due to lower gas permeability.

Here, the cathode loss factors of the bundle were calculated for different R_{cell}, 0.5 and 0.3 Ωcm^2 (set for higher power output, higher operating temperature). Fig. 9 shows the cathode loss factor of the bundle (LSCF20) as a function of distance (L) between tubes for three operating consitions, $R_{cell} = 1.01$, 0.5, 0.3 Ωcm^2 at $D = 1$ mm. For these calculations, the conductivity of the cathode matrix was assumed to be the same (Table 1). As can be seen, it was shown that the cathode loss factor increased as L decreased, as well as high power output conditions (low R_{cell}) resulted in larger cathode loss factor. Thus, this fact needs to be carefully considered to determine the arrangement of the tubular cells in the cathode matrix for cube bundles and stacks.

Currently, integration technology of the tubular SOFC bundles is examined to obtain higher output voltage. Fig. 10 shows the design of a 72 V output stack module with the volume (exclude manifold) of 30 cc stack volume, which is expected to perform 30 W at 48 V maximum output under 500 °C operating temperature. This bundle design allows stacks to perform any output power, and voltage, and therefore, use of the SOFC bundles for stack fabrication could be useful especially for portable SOFC systems.

5. Conclusions

A newly developed tubular SOFC stack which consists of three tubular SOFC bundles was proposed and fabricated. The performance was shown to be ~2.8 V (OCV) and 1 W at 1.6 V under 500 °C operating temperature with the stack volume of less than 1 cm^3. These results were obtained by newly developed fabrication technology of the bundle/stack and optimization of the design of the tubular SOFCs and the cathode matrix. The cathode loss factor due to the resistance of the cathode matrix was defined and calculated as a function of distance between tubes to optimize the bundle design. The cathode loss factor, effect of the cathode matrix as a current collector, was estimated to be less than 0.01 at 484 °C operating temperature. The calculation also suggested that careful consideration was needed for the design of the bundle. Currently, further accumulation of the tubular SOFC bundles are considered to obtain higher output voltage and power at various operating temperatures. It was shown that the new bundles were useful to design any sized SOFC systems, especially for portable devices.

Acknowledgment

This work had been supported by NEDO, as part of the Advanced Ceramic Reactor Project.

References

[1] O. Yamamoto, Electrochim. Acta 45 (2000) 2423.
[2] N.Q. Minh, J. Am. Ceram. Soc. 78 (1993) 563.
[3] S.C. Singhal, Solid State Ionics 152–153 (2002) 405.
[4] S. de Souza, S.J. Visco, L.C. DeJohnge, J. Electrochem. Soc. 144 (1997) L35.
[5] A.V. Virkar, J. Chen, C.W. Tanner, J.W. Kim, Solid State Ionics 131 (2000) 189.
[6] B.C.H. Steele, Mater. Sci. Eng. B 13 (1992) 79.
[7] T. Ishihara, H. Matsuda, Y. Takita, Solid State Ionics 79 (1995) 147.
[8] H.G. Bohn, T. Schober, J. Am. Ceram. Soc. 83 (2000) 768.
[9] Z. Shao, S.M. Haile, Nature 431 (2004) 170–173.
[10] B.C.H. Steele, Solid State Ionics 129 (2000) 95.
[11] K. Kuroda, I. Hashimoto, K. Adachi, J. Akikusa, Y. Tamou, N. Komado, T. Ishihara, Y. Takita, Solid State Ionics 132 (2000) 199.
[12] S.P. Yoon, J. Han, S.W. Nam, T.H. Lim, I.H. Oh, S.A. Hong, Y.S. Yoo, H.C. Lim, J. Power Sources 106 (2002) 160.
[13] B.C.H. Steele, A. Heinzel, Nature 414 (2001) 345–352.
[14] S.P. Simner, J.F. Bonnett, N.F. Canfield, K.D. Meinhardt, V.L. Sprenkle, J.W. Stevenson, Electrochem. Solid State Lett. 5 (2002) A173.
[15] H. Huang, M. Nakamura, P.C. Su, R. Fasching, Y. Saito, F.B. Prinz, J. Electrochem. Soc. 154 (1) (2007) B20–B24.
[16] K. Eguchi, T. Setoguchi, T. Inoue, H. Arai, Solid State Ionics 52 (1992) 165.
[17] T. Hibino, A. Hashimoto, K. Asano, M. Yano, M. Suzuki, M. Sano, Electrochem. Solid State Lett. 5 (2002) A242.
[18] J. Yan, H. Matsumoto, M. Enoki, T. Ishihara, Electrochem. Solid State Lett. 8 (8) (2005) A389–A391.
[19] N.M. Sammes, Y. Du, Int. J. Appl. Ceram. Technol. 4 (2) (2007) 89–102.
[20] N.M. Sammes, Y. Du, R. Bove, J. Power Sources 145 (2005) 428–434.
[21] K. Kendall, M. Palin, J. Power Sources 71 (1998) 268–270.
[22] K. Yashiro, N. Yamada, T. Kawada, J. Hong, A. Kaimai, Y. Nigara, J. Mizusaki, Electrochemistry 70 (12) (2002) 958–960.
[23] P. Sarkar, L. Yamarte, H. Rho, L. Johanson, Int. J. Appl. Ceram. Technol. 4 (2) (2007) 103–108.
[24] T. Suzuki, T. Yamaguchi, Y. Fujishiro, M. Awano, J. Power Sources 163 (2006) 737–742.
[25] Y. Funahashi, T. Shimamori, T. Suzuki, Y. Fujishiro, M. Awano, ECS Trans. 7 (1) (2007) 643–649.
[26] T. Suzuki, Y. Funahashi, T. Yamaguchi, Y. Fujishiro, M. Awano, Electro. Electro. Solid State Lett. 10 (2007) A177.
[27] L.W. Tai, M.M. Nasrallah, H.U. Anderson, D.M. Sparlin, S.R. Sehlin, Solid State Ionics 76 (1995) 273.
[28] Y.J. Leng, S.H. Chan, S.P. Jiang, K.A. Khor, J. Power Sources 170 (2004) 9–15.
[29] E.D. Wachsman, Solid State Ionics 152–153 (2002) 657.
[30] Y. Xiong, K. Yamaji, N. Sakai, H. Negishi, T. Horita, H. Yokokawa, J. Electrochem. Soc. 148 (2001) E489.
[31] A. Tomita, S. Teranishi, M. Nagao, T. Hibino, M. Sano, J. Electrochem. Soc. 153 (6) (2006) A956–A960.
[32] R.T. Leah, N.P. Brandon, P. Aguiar, J. Power Sources 145 (2005) 336.